*Materials Research*. 2022; 25:e20210463
DOI: https://doi.org/10.1590/1980-5373-MR-2021-0463

# Kinetics of the UNS S32750 Super Duplex Stainless Steel Low-Temperature Plasma Nitriding

***J. F. V. Lima*[a], *C. J. Scheuer*[a,b]*, *S. F. Brunatto*[a,c], *R. P. Cardoso*[a,d]**

[a]*Grupo de Tecnologia de Fabricação Assistida por Plasma e Metalurgia do Pó, Curitiba, PR, Brasil.*
[b]*Universidade Federal de Santa Maria (UFSM), Departamento de Engenharia Mecânica (DEM), Santa Maria, RS, Brasil.*
[c]*Universidade Federal do Paraná (UFPR), Departamento de Engenharia Mecânica (DEMEC), Curitiba, PR, Brasil.*
[d]*Universidade Federal de Santa Catarina (UFSC), Departamento de Engenharia Mecânica (EMC), Florianópolis, SC, Brasil.*

Received: September 14, 2021; Revised: March 05, 2022; Accepted: March 06, 2022

This work reports an experimental investigation on the thermodynamic and kinetic view-point of the nitrided layer growth behavior, carried out separately at ferrite and austenite phase grains, for the UNS S32750 super duplex stainless steel (SDSS). For this purpose, and motivated by the DSSs distinct behavior showing formation of two- or single-phase nitrided layers, which apparently depend on the steel substrate chemical composition, two series of treatment were studied here, one varying the nitriding temperature on the 300-450 °C range for 4 h time, and other one varying the time on the 2-8 h range at 350 °C. Microstructural characterization of studied layers by means of SEM and EDS analysis, XRD and microhardness measurements showed precipitation-free nitrogen-expanded austenite layer formation on both steel phases for all samples treated up to 400 °C. The nitriding kinetics study showed that the layer thickness on both steel phases is proportional to the square root of the treatment time and follows an Arrhenius law for the studied treatment temperatures. The nitrogen diffusion activation energy, separately determined from the layer growth on each steel phase, was 115±3.2 and 120±5.4 kJmol$^{-1}$, for austenite and ferrite grains, respectively.

**Keywords:** *UNS S32750 super duplex stainless steel, low-temperature nitriding, nitriding kinetics, plasma nitriding, nitrogen-expanded austenite.*

## 1. Introduction

Duplex stainless steels (DSSs) have been extensively used in several industrial segments, like shipbuilding, offshore, chemical, paper and pulp, petrochemical, desalination plants and oil and gas, where high corrosion resistance (namely pitting, crevice and stress corrosion resistance) and significant mechanical properties, conferred by its ferritic-austenitic structure, are required[1]. DSSs typically contain, in wt. %, 18.5-27 Cr, 4-8 Ni and 2-6 Mo and have, while solution-treated, ferrite-austenite (half to half) microstructure with preferential partitioning of chromium and molybdenum in ferrite (α) grains, and nickel in austenite (γ) grains[2]. One reason for the growing research and development interest in DSSs lies in the fact that they tend to be ideal materials for use in marine engineering equipment[3-5]. Allied to it, DSSs present good potential to replace the costly nickel-based and corrosion-resistant alloys, like austenitic stainless steels (ASSs) that typically contain 8-30 wt.% Ni in its compositions, mainly due to the strong nickel market price volatility[1]. This explains why the production of DSSs tends to grow at the expense of a decrease in the production of ASSs[6]. On the other hand, despite of good overall properties, DSSs tends to present low wear resistance, thus weak tribological behavior[7], which is limiting factor for expanding their use.

In applications where surface properties are important, surface treatments constitute an attractive technological tool to improve the DSSs tribological behavior, increasing the components lifespan[8]. The benefits of the nitrogen-alloying by plasma treatments at the surface of ferritic[9,10] as well as austenitic[11-15] stainless steels are well established. In contrast, the response of the DSSs to plasma nitriding was less explored, being far from completely understood, deserving additional research efforts. The existing research indicates that the application of nitriding temperatures above 500 °C, promote the formation of Cr and Fe nitrides, increasing the DSSs hardness and wear resistance, but reducing their corrosion resistance[16]. In its turn, the application of low-temperature (paraequilibrium) nitriding, typically performed below 450°C, enables the obtainment of chromium nitride precipitation-free hardened surfaces, presenting a nitrogen-expanded supersaturated structure, which displays better performance to failure by corrosion and wear when compared to non-nitrided material[17-20].

Table 1 presents a compilation of the main papers on the literature about the low-temperature plasma nitriding (LTPN) of DSSs[7,8,17-28]. Regarding the nitrided layer formation

*e-mail: cristiano.scheuer@ufsm.br

**Table 1.** Summary of the main contributions found in the open literature on low-temperature nitriding of duplex stainless steels.

| References | Nitriding technique | Duplex stainless steel | Nitriding condition | | Main results |
|---|---|---|---|---|---|
| | | | Time (h) | Temperature (°C) | |
| Pinedo et al.[7] | d.c. | UNS S31803 | 20 | 400 | Formation of a two-phase $\gamma_N + \alpha_N$ layer with 3.8 and 4.4 wt.% N, respectively ($\alpha_N$ thicker than $\gamma_N$, both with microhardness > 1350 HV). |
| Tschiptschin et al.[8] | d.c. | UNS S31803 | 20 | 400 | Formation of a two-phase $\gamma_N + \alpha_N$ layer, with 3.0 and 2.5 μm thickness, and 1360 HV and 1510 HV microhardness, respectively (intense coherent ε-$Fe_3N$ nitride precipitation inside $\alpha_N$). |
| Larisch et al.[16] | Gas nitriding | UNS S31803 | 3 to 12 | 400 to 550 | Formation of a two-phase $\gamma_N + \alpha_N$ layer formed in austenite and ferrite grains, respectively. |
| Calabokis et al.[17] | d.c. (LTPN) | UNS S32750 | 4 | 350, 400 | Formation of a precipitation-free single-phase $\gamma_N$ layer with significant corrosion resistance performance improvements for all treatment conditions. |
| Bielawski and Baranowska[18] | d.c. | UNS S31803 | 8 to 60 | 250 to 500 | Formation of precipitation-free single-phase $\gamma_N$ layer, with thickness of 15 μm and 8.9 wt.% N produced at temperatures up to 400 °C. |
| Kliauga and Pohl[19] | high-frequency pulsed plasma | UNS S31803 | 20 and 40 | 350 and 400 | At 350 °C, the layer homogeneously covers the ferrite and the austenite phase regions, the latter phase showing $\gamma_N$ formation, and needle-like α″-$Fe_{16}N_2$ precipitation occurring in the layer-ferrite phase interface. At 400°C, $Cr_2N$ + $Fe_{2-3}N$ + γ'-$Fe_4N$ nitrides were present in the layer showing cracks. |
| Blawert et al.[20] | PI[3] | UNS S31803 | 3 | 400 | The pre-existing ferrite phase transforms into $\gamma_N$ phase, which in the extreme surface decomposes into ferrite + martensite + CrN. |
| Li et al.[21] | d.c. | UNS S82441 | 10 | 390 to 480 | The original austenite phase become $\gamma_N$ phase, and the ferrite phase is supersaturated with N forming ε-$Fe_3N$ nitride precipitates. |
| Chiu et al.[22] | ASPN | UNS S31803 | 10 to 25 | 400 to 450 | At 420 °C, a two-phase $\gamma_N$ and $\alpha_N$ layer is formed, and at 435 and 450 °C, Fe and Cr nitrides precipitate in the layer. |
| Nagatsuka et al.[23] | ASPN and d.c. | UNS S32550 | 5 | 400 and 450 | Single-phase $\gamma_N$ layer is obtained (in austenite as well as in ferrite phases) on both d.c. and ASPN samples treated at 400 and 450 °C. |
| Alphonsa et al.[24] | d.c. | UNS S32205 | 4 | 350 to 500 | GIXRD results show that at 350 and 400°C only $\gamma_N$ phase is present in the layer and that at 450 and 500 °C $Fe_3N$ and CrN phases form. |
| Assmann et al.[25] | GDN and CIBNI | UNS S32101 | 3 | 300, 350 and 380 | A $\gamma_N$ layer with nitride precipitation arising from 300 °C, with 1220 HV microhardness is obtained for the poor nitrogen atmosphere GD process. The CIBNI process even at high temperature produced only nitrogen-expanded austenite. |
| Blawert et al.[26] | PI[3] | UNS S31803 | 1, 3 and 7 | 200,400 and 500 | Single-phase $\gamma_N$ layer is formed on both austenite and ferrite grains. |
| Oliveira et al.[27] | PI[3] | UNS S32750 | 3 | 292 to 401 | ε-$Fe_{2-3}N$ and γ-$Fe_4N$ iron nitrides are formed in the modified ferrite grains, whereas $\gamma_N$ was produced mostly in austenite grains. Overall near surface microhardness is increased from 610 to 1530 HV. |
| Bobadilla and Tschiptschin[28] | d.c. | UNS S31803 | 4 | 350 to 500 | The non-unidirectional N diffusion tends to result in a N diffusion flow from ferrite to austenite, leading to the formation of a duplex $\gamma_N + \alpha_N$ layer with small thickness difference in both phases. |

d.c.: direct current; PI[3]: plasma immersion ion implantation; ASPN: active screen plasma nitriding; GDN: glow discharge nitriding; and CIBNI: conventional ion beam nitrogen implantation.

mechanisms and its phase constitution, a portion of these research point out that treated layer is constituted of a two-phases $\gamma_N$ (nitrogen-expanded austenite) and $\alpha_N$ (nitrogen-expanded ferrite) structure[7,8,21,22,27,28]; whereas other portion claim that treated surface is formed by a single-phase $\gamma_N$ layer[16,17,20,23,24,26]. The two-phase structure formation would be due to the nitrogen enriching both the austenite and ferrite phases, but with no change on its respective stabilities, whereas the single-phase $\gamma_N$ layer formation would be due to the nitrogen content enhancement leading the austenite phase stability to be attained also in ferrite grains. Regarding the treatment temperature limit values to prevent chromium

nitride precipitation, some authors[8] claim that the Cr-nitride phases precipitation occurs for nitriding temperatures from 400°C, others[10] show that this only happens for nitriding temperatures above to 450 °C. One can note that the steel type, processing conditions, and the applied technique can lead to significantly different results regarding these aspects.

It is also to be noted that the UNS S32750 SDSS, studied here, presents a high 'Pitting Resistance Equivalent Number' (PREN = wt.% Cr + 3.3 × wt.% Mo + 20 × wt.% N), in the case higher than 40[29], which makes it a material indicated for extremely corrosive environments. As seen from the above-indicated PREN equation, by alloying the UNS S32750 SDSS surface with nitrogen better corrosion resistance should be expected, according to ref[3].

Using a strong metallurgical background and the knowledge produced up to now on low-temperature nitriding of stainless steels, the aim of the present work was to conduct experiments to study the nitriding process kinetics of UNS S32750 SDSS substrates, bringing a deeper discussion on determining factors that influence the treatment on both steel phases. Considering that the chemical composition of the substrate plays important role on the layer formation in thermochemical treatments of different stainless steels[30,31], this same premise should be also valid for each phase of DSSs and SDSSs, which present different compositions and structures. So, this work reports an experimental investigation on the thermodynamic and kinetic view-point of the nitrided layer growth behavior, carried out separately at the ferrite and austenite phase grains for the UNS S32750 super duplex stainless steel (SDSS), as a function of the nitriding temperature and time.

## 2. Experimental Procedure

Samples of the UNS S32750 SDSS, with 20 × 20 × 3 $mm^3$, were cut by wire electrical discharge machining from a 2.5-inch rolled steel rod. Semi-quantitative X-ray fluorescence analysis was used to determine the samples chemical composition, which showed 25.6% Cr, 6.8% Ni and 4.1% Mo (in wt.%). Samples were grinded and polished with 1 μm $Al_2O_3$ abrasive suspension and 1 μm diamond paste to obtain a mirror polished finishing. Before nitriding, samples were cleaned in ultrasonic bath using isopropyl alcohol, dried in a heated airflow and introduced into the discharge chamber. The treated surfaces were always those perpendicular to the rod rolling direction. The average microhardness values obtained in the ferrite and austenite grains for untreated samples were 325 and 270 HV0.01, respectively.

Plasma nitriding was carried out in the same plasma system previously illustrated in Anjos et al.[32]. The plasma apparatus consisted basically of a square-wave pulsed DC power supply operating at 4.16 kHz, and a stainless steel discharge chamber of 350 × 380 mm (diameter × height), attached to steel plates and sealed with O-rings at both ends. In such system, sample heating was reached by plasma species (ions and fast neutrals) bombardment, being the samples temperature measured by means of a chromel–alumel thermocouple (K–type of 1.5 mm diameter) inserted 8 mm depth into the sample holder (see Anjos et al.[32]).

After evacuating the system to a residual pressure of 3 Pa (22 mTorr) using a double stage mechanical vacuum pump, samples were negatively biased at the voltage of 700 V in order to perform its (plasma) sputter-cleaning. This nitriding steps was performed at 300 °C, for 0.5 h, using a gas mixture constituted of 80% $H_2$ + 20% Ar, at a flow rate of 3.34 × $10^{-6}$ $N.m^3.s^{-1}$ (200 sccm), under 400 Pa (3 Torr) pressure. Two treatment series were studied aiming to determine the influence of the temperature and time parameters on the nitriding kinetics:

i. one varying the nitriding temperature at 300, 350, 400 and 450 °C for 4 h; and,
ii. the other one varying the nitriding time for 2, 4 and 8 h, at a fixed temperature of 350 °C.

In both series the treatments were performed employing a gas mixture constituted by 70% $N_2$ + 20% $H_2$ + 10% Ar, and the other parameters being kept at the same values as those used in the cleaning step. It is important to clarify that the higher nitriding temperature (450 °C) and longer time (8 h) parameters were chosen taking care to avoid the "475°C tempering embrittlement" in the studied steel.

For the microstructural characterization of the treated surfaces, polished samples cross-sections were etched using Behara reagent (20 ml hydrochloric acid + 80 ml distilled water + 1 g potassium metabisulfite + 2 g ammonium bifluoride). Microstructures were observed using a scanning electron microscope (SEM), in the case a TSCAN VEGA 3 apparatus equipped with energy dispersive X-ray microprobe (EDS) to carry out elemental analyses. The phases of the obtained layers were identified by means of X-ray diffractometry (XRD), using a Shimadzu XRD 7000 diffractometer with CuKα radiation ($K\alpha_1 \rightarrow \lambda = 1.54056$ Å and $K\alpha_2 \rightarrow \lambda = 1.54439$ Å), in the Bragg-Brentano (for 2θ angle varying on the 30–90° range) XRD configuration, using a scanning speed of 2°/min. Hardness measurements were performed on the treated (top of the sample) and untreated (bottom of the sample – not exposed to plasma) surfaces using a Shimadzu microdurometer type HMV-2 T, applying a load of 10 gf (9.8 × 10− 2 N), for a peak-load contact of 15 s. To be representative, due to the relatively large distribution of the measurement values in different phases, the layer thickness and microhardness values were obtained from the mean of fifteen measurements taken for grains of each phase.

Finally, the activation energy for the nitrogen diffusion into the treated layer was determined by the Arrhenius plot for both austenite and ferrite phases, following the procedure described in ref[28,33,34]. From the Arrhenius-type behavior for the nitriding thickness data, considering that the process is diffusion controlled (being the layer thickness proportional to $(Dt)^{1/2}$, where $D$ is the diffusion coefficient and $t$ is the diffusion time), the activation energy ($Q_d$) for nitrogen diffusion can be calculated by the slope of the Arrhenius plot according to Equation 1:

$$\ln \xi = A - \left(\frac{Q_d}{2R}\right).\frac{1}{T} \quad (1)$$

where ξ is layer thickness (μm), $R$ is the universal gas constant (8.31 J $mol^{-1}K^{-1}$), and T corresponds to absolute temperature (K).

## 3. Results and Discussion

### *3.1. Effect of the variation of the nitriding temperature*

Cross-section micrographs of samples treated at 300, 350, 400 and 450 °C, for 4 h are presented in Figure 1a-d, respectively (As an additional support optical micrographs are also presented in Figure A1a-d of Appendix A). A continuous layer formed from the nitrogen diffusion in both steel phases can be observed for all studied conditions. As expected, thicker layers are obtained for higher treatment temperatures (also see Figure 2). Note that the original austenite and ferrite grains as well as the obtained layers have different reactivity to the Behara reagent chemical etching. Two distinct region kinds can be easily observed, as follows (see Figure 1a-d):

i. a nitrogen-chemically-altered region at the effectively treated surface, where the obtained layer (of light gray-aspect) is more resistant to etching than the other regions; and,
ii. a non-chemically-altered region, at the substrate bulk, which can be subdivided in two other regions clearly showing the original steel phases, namely the ferrite grains (of dark-aspect) much more susceptible to etching, and the austenite grains (of gray-aspect) slightly less susceptible to etching.

This result is especially important in the present work, since the revealed microstructure is strong enough to identify and distinguish at least three different phases in the studied samples. In this case, the continuous layer in the nitrogen-chemically-altered region seems to be very homogeneous when formed on both the ferrite grains and the austenite grains, presenting totally different aspect

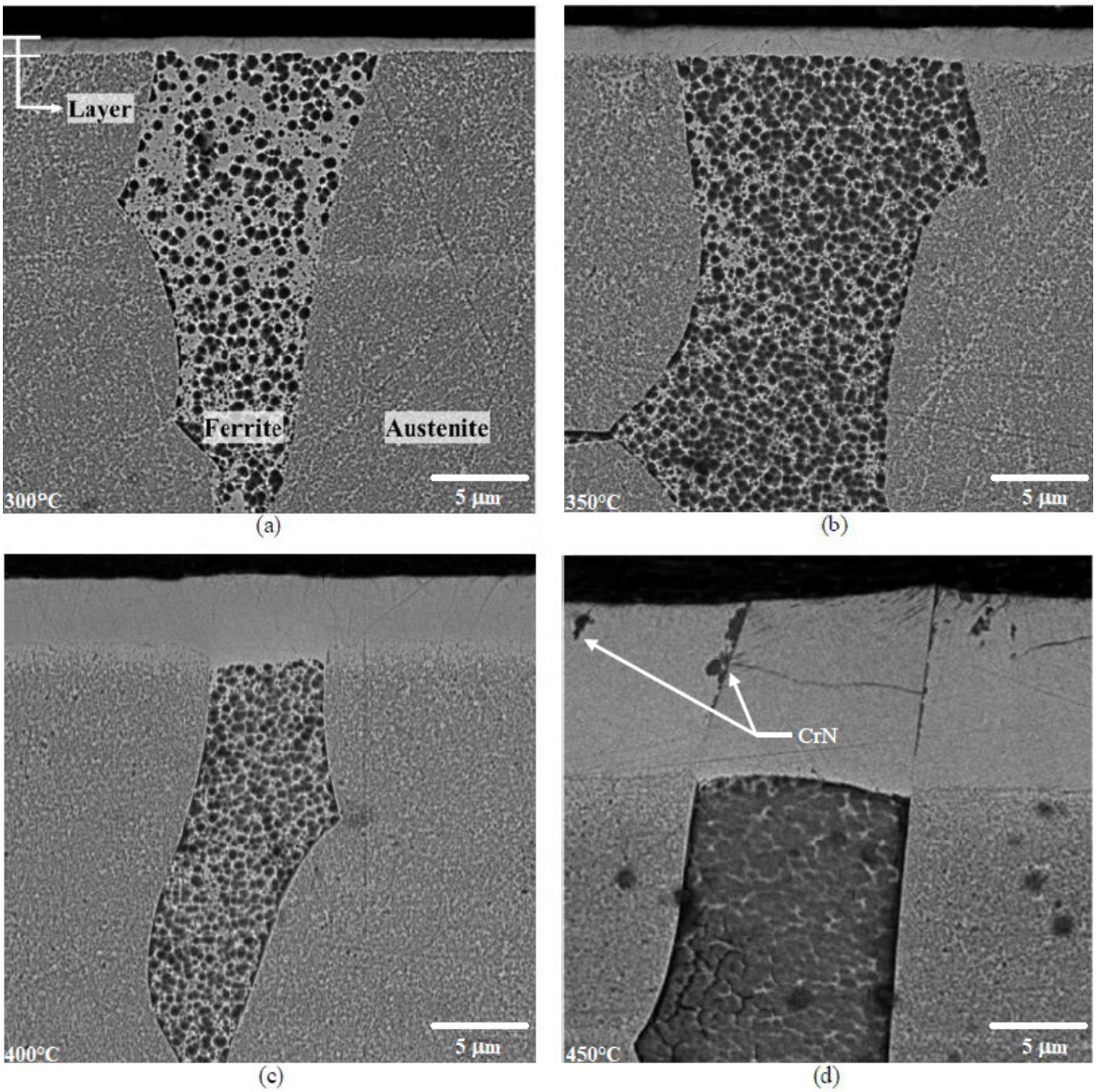


**Figure 1.** Cross-section SEM micrographs of samples treated at: (a) 300, (b) 350, (c) 400, and (d) 450 °C. Treatments carried out for 4 h, using a gas mixture composed of 70% $N_2$ + 20% $H_2$ + 10% Ar at a flow rate of $3.34\times10^{-6}$ $Nm^3s^{-1}$, and pressure of 400 Pa.

regarding the original steel phases (valid for samples treated at 300, 350 and 400 °C in Figure 1a-c, respectively). This result suggests that the continuous layer obtained in the nitrogen-chemically-altered region is constituted of a unique phase. Differently, the aspect of the 450 °C treated layer in Figure 1d additionally suggests precipitation of Cr-nitride phase along the nitrided layer formed over the ferritic and austenitic grains, agreeing with the indicated in ref[20,35]. It is important to highlight that, unlike what was shown here, other authors[18,22,24] reported the occurrence of Cr-nitride precipitation only in the ferritic grains, for similar treatment temperatures. Since CrN precipitation is incipient, CrN is not directly observed. The observed regions are sites depleted in chromium, due to CrN precipitation, which are less chemically resistant to the Behara etchant.

The Arrhenius plot for the thickness of the layer formed on each phase is depicted in Figure 2. These data were elaborated considering that nitrogen diffusion is the limiting factor for the layer growth, and so, the obtained activation energy is considered representative of nitrogen diffusion in the treated layer. Even if it is good approximation, it is to be noted that, strictly speaking, the obtained values are in fact and effective activation energies since, for example, the N surface concentration is not the same for the different temperatures. From Figure 2 results, it can be observed that the obtained layer on the ferrite phase is slightly thicker than that on the austenite phase. Despite the well-known relationship between diffusion and crystalline structure and orientation[36], this argument alone is not sufficient to explain this result, regarding the nitrogen diffusion in DSSs, as it will be presented ahead considering at least three other different factors. The observed data linearity in the plot suggests that the LTPN of the UNS S32750 SDSS is a diffusion-controlled process and that atomic diffusion is the limiting mass transfer mechanism for the treated layer growth. It also suggests that the secondary phase precipitation did not significantly influence the process activation energy. Some authors[28-34] show a deviation from the linearity for high temperature treatment conditions, indicating that the layer growth is affected by the secondary phase precipitation, leading to the increase of the activation energy needed for the layer growth. Although Figure 1d indicates the treated layer sensitization occurrence, thus Cr-nitride precipitation, it is believed that it was only in its initial stage, since it did not significantly interfere on the nitriding process kinetics.

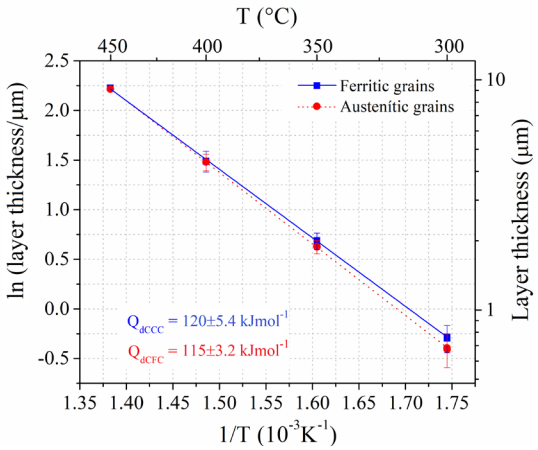


**Figure 2.** Arrhenius plot for the plasma nitrided layer thickness formed on austenite and ferrite grains of the UNS S32750 SDSS. Treatments carried out for 4 h, using a gas mixture composed of 70% $N_2$ + 20% $H_2$ + 10% Ar at a flow rate of $3.34\times10^{-6}$ $Nm^3s^{-1}$, and pressure of 400 Pa.

The activation energy for the nitrogen diffusion into the treated layer formed on the austenite and ferrite grains, estimated by the Arrhenius plot slope (Figure 2), was 115±3.2 and 120±5.4 kJmol$^{-1}$ (equivalent to 1.19±0.03 and 1.24±0.05 eV, and to 27.5±0.7 and 28.7±1.3 kcal/mol), respectively. This slight difference in the obtained activation energies gives additional support to the assumption that a single-phase layer has been formed on both the phases, being this slight difference probably related to specific characteristics of the treated layer on each substrate phase kind, as discussed ahead. These activation energies agree very well with those of Bobadilla and Tschiptschin[28], which obtained values of 117 and 124 kJmol$^{-1}$ for the nitrogen diffusion activation energies in UNS S31803 DSS austenite and ferrite grains, respectively, but, differently from here, they suggest the obtainment of a two-phase nitrided layer. Results published in the literature indicate nitrogen diffusion activation energy values of 111.4 kJmol$^{-1}$ for PIM 316L ASS[37] and 107 kJmol$^{-1}$ for AISI 304L ASS[38]. For ferritic stainless steels, no activation energy data were found in the literature, but much earlier, a study presented an activation energy of 76 kJmol$^{-1}$ for a low-alloyed ferrite (α-Fe) steel[39].

Starting from the data determined by the Arrhenius plot extrapolation and considering Equation 1, the evolution of the nitrided layer as a function of the treatment temperature in the austenitic grains of the UNS S32750 SDSS can be described by Equation 2, whereas that for ferritic grains, through Equation 3:

$$\ln \xi\left(K/\mu m\right) = 2.49 - \frac{115\,kJmol^{-1}}{2R}\cdot\frac{1}{T} \quad (2)$$

$$\ln \xi\left(K/\mu m\right) = 2.46 - \frac{120\,kJmol^{-1}}{2R}\cdot\frac{1}{T} \quad (3)$$

The higher thickness of the nitrided layer on the ferrite phase, according to ref[8,16,17,27,36,37], is justified by the higher nitrogen diffusion coefficient in the ferrite than in the austenite structure. In the present work, this justification makes sense only for the initial nitriding moments, when the nitrogen enrichment was not sufficient to promote the ferrite-to-austenite transformation. This seems to be true up to the moment the nitrogen-supersaturated ferrite would transform to nitrogen-alloyed austenite, which is believed to occur in accordance with XRD results presented ahead (see Figure 3). Finally, from Figure 1a-d it is also possible to verify a slight tendency to a more prominent layer growth at the original grain boundaries between ferrite and austenite phases. Since these boundaries are high diffusivity paths that presents lower diffusion activation energy[40], such sites would facilitate the nitrogen diffusion and can explain the observed tendency.

Going further in the discussion, it is worth explaining the meaning of the activation energy regarding the specific atomic migration event that would be operating in the present

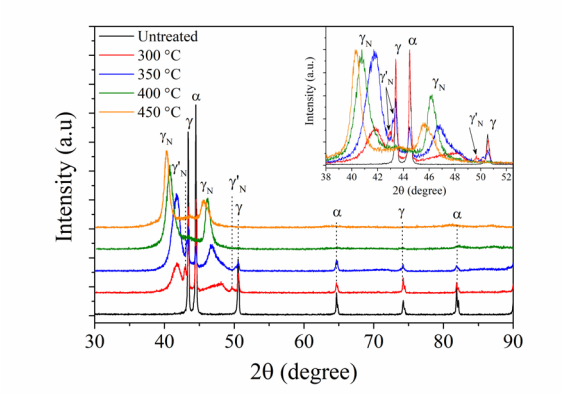


**Figure 3.** XRD patterns for untreated sample and samples treated at 300, 350, 400 and 450 °C. Treatments carried out for 4 h, using a gas mixture composed of 70% $N_2$ + 20% $H_2$ + 10% Ar at a flow rate of $3.34\times10^{-6}$ $Nm^3s^{-1}$, and pressure of 400 Pa. (where: γ – austenite phase; α – ferrite phase; $\gamma_N$ – nitrogen-expanded austenite phase; and $\gamma'_N$ – secondary nitrogen-expanded austenite phase.

treatment. As known, the nitrogen atoms migration is based on the interstitial diffusion mechanism, but the involved activation energy can be dependent on the environment where such atoms are diffusing, thus on the layer composition. This point is especially important here, since the studied stainless steel substrate presents two phases, with different compositions depending on the grain (phase) kinds. As the thermochemical treatment is performed in paraequilibrium the substrate substitutional alloying elements will not significantly diffuse during treatment. So, even if an expanded-austenite treated layer is formed over both grain kinds, the composition of the treated layer built on the different phases will be different, as a consequence of the substitutional alloying elements partition occurred during the steel production (see factor *i*, below). As soon, although the activation energy values calculated here for each phase are similar, the hypothesis is supported that different phenomena are involved and promote the formation of the nitrided layer in each of these phases, as discussed below.

On the other hand, regarding the point lattice defects produced from the plasma-surface interaction, besides the gradient of the nitrogen interstitial, new supposedly produced vacancies would mainly work on the first atomic layers of the treated material. Since the vacancy density gradient tends to rapidly decrease into the substrate bulk, it would be important for the increment of the nitrogen solubility at the outermost surface of the substrate. It is to be remembered that in low-temperature (paraequilibrium) nitriding of stainless steels, the substitutional diffusion mechanism that is strongly dependent on the equilibrium vacancy density, would be negligible.

Therefore, the nitrogen diffusion in treated surfaces of DSSs, besides depending on each phase crystalline lattice structure, would also depend on at least four more factors:

i. The partitioned alloying elements effect on the nitrogen diffusivity: Ni atoms partitioned in austenite grains, and Cr and Mo[1] atoms preferentially partitioned in ferrite grains[2], influence the nitrogen interstitial atom diffusion kinetics, as indicated is ref[30,31]. It has been shown that Ni in MSSs promotes the layer thickness reduction in paraequilibrium nitriding[30]. More, the nitrogen solubility decreases as the Ni content on Fe alloys is increased[41]. So, one can assume that the nitrogen diffusion in the treated layer formed on the ferrite is faster than in austenite;
ii. The alloying elements trapping effect: diffusion or trap sites are usual positions occupied by interstitial atoms diffusing into SSs at low temperature[42]. Nitrogen easily diffuses from diffusion sites due to its lower activation barrier (1.45 eV[43]), but it has difficulty to diffuse from trap sites, showing greater activation barrier (2.5 eV[43]), due to Cr atoms. Thus, as Cr as well as Mo atoms are preferentially in ferrite grains[2], it is assumed that a higher nitrogen diffusion activation energy in the treated layer on ferrite grains is due to the trapping effect;
iii. The different stress generated in both phases of DSSs: during heating, in the initial stage of the samples treatment, different expansion coefficients of ferrite and austenite phases tend to result in compressive residual stresses in ferrite, while equilibrium tensile stresses are generated in the austenite[44]. Tensile stresses promote a decrease on the activation energy for interstitial atoms diffusion[45], whereas compressive stress can retard its fast diffusion[46], opposing, at least in part, the factor *i*. So, it is assumed that at the beginning of the treatment nitrogen diffusion in the austenite phase, subjected to tensile stress, is faster than in ferrite grains that are subjected to compressive stress. Considering that the nitrogen-alloyed layer is constituted of expanded-austenite, the phase transformation energetic barrier in original ferrite grains must be overcome to initiate the layer growth; and
iv. The stress resulting from ferrite-to-austenite transformation due to nitrogen supersaturation: After being supersaturated by nitrogen atoms, the ferrite structure in the treated layer is transformed in expanded-austenite ($\gamma_N$). The present factor is corroborated by results published in ref[47,48]. In Allenstein et al.[47], strong evidences of tempered martensite (or *bcc* structure ferrite)-to-nitrogen-expanded austenite transformation was observed in CA6NM MSS steel after LTPN. In Zangiabadi et al.[48], conclusive evidence for martensitic nature phase isothermal transformation from martensite/ferrite-to-austenite was observed at paraequilibrium temperature nitriding (LTN) of 15-5 PH (precipitation hardening), 17-7 PH, and 2205 (duplex) stainless steel surfaces with nitrogen concentrations from 8 to 16 at.%[48]. Since the ferrite-to-austenite transformation occurs with volumetric contraction[49], an eventual tensile

[1] Molybdenum could also promote the trapping effect but, since chromium has superior affinity to nitrogen and is present in higher concentration in DSSs, authors suppose that its effect is mainly related to the lattice distortion.

residual stress state at the transformed surface would contribute to a greater nitrogen diffusivity. It is to be remembered that the cause of the volume and packing density differences for both the considered iron (phases) crystalline structures is also related to other factors such as the coordination number, this one affecting the effective atomic (and of radii) ratios, besides the possible different spin electronic states, much more than simply on those results obtained from the hard sphere model.

From our results, it seems that factors *iii* and *iv* influence the nitrogen diffusion and alloying through the layer formed on the ferrite phase, leading its structure and composition to be changed along the treatment time and surely all over the treated layer depth, remembering that factors *i* and *ii* remain unchanged in this case, since the substitutional atoms diffusion is negligible in paraequilibrium[19]. Based on all above-presented aspects, even that factors *ii* and *iii* tend to promote an activation energy increase for the layer built in the ferrite phase, allied to the similar role promoted by the higher molybdenum atoms in this phase[31,45], as confirmed ahead (see Figure 4 and Table 2 results), the nitrogen-supersaturated ferrite-to-austenite transformation would explain the similar layer growth activation energy values obtained in our work on both phases as well as the similar treated layer growth rates observed in both phases after the referred transformation. This also should hold for all nitriding process of DSS where this transformation occurs and that is limited by the N atoms diffusion kinetics. This assumption is supported by observing treated layer thickness values indicated in Figure 2. Regarding the diffusion in austenite grains, its higher chromium and molybdenum contents in the UNS S32750 SDSS when compared to that found in the AISI 316[37] and AISI 304[38] ASSs would also lead the nitrogen diffusion activation energy in the SDSS austenite phase to be slightly higher than that in ASSs.

Figure 3 presents XRD patterns of untreated and treated samples. Patterns for untreated samples show only peaks referred to ferrite and austenite phases, as expected. XRD patterns of treated samples show the occurrence of nitrogen-expanded austenite ($\gamma_N$ / $\gamma'_N$) phase peaks, thus strongly suggesting the single-phase expanded-austenite ($\gamma_N$) layer formation. Note that the $\gamma_N$ phase peaks are asymmetric, probably due to the depth nitrogen compositional gradient, varying from surface into the substrate bulk. Broadened and reduced-intensity diffraction peaks due to crystalline lattice

**Table 2.** EDS elemental analysis characterization of the nickel (austenite-stabilizer), and chromium and molybdenum (ferrite-stabilizer and stable nitride formers alloying elements) partition on non-treated UNS S32750 SDSS samples.

| Phase | Ni / Cr / Mo (wt.%) | Ni / Cr / Mo (at.%) |
|---|---|---|
| Austenite | 8.5 / 24 / 5.5 | 8.1 / 26 / 3.2 |
| Ferrite | 5.5 / 27 / 7.0 | 5.2 / 29 / 4.0 |

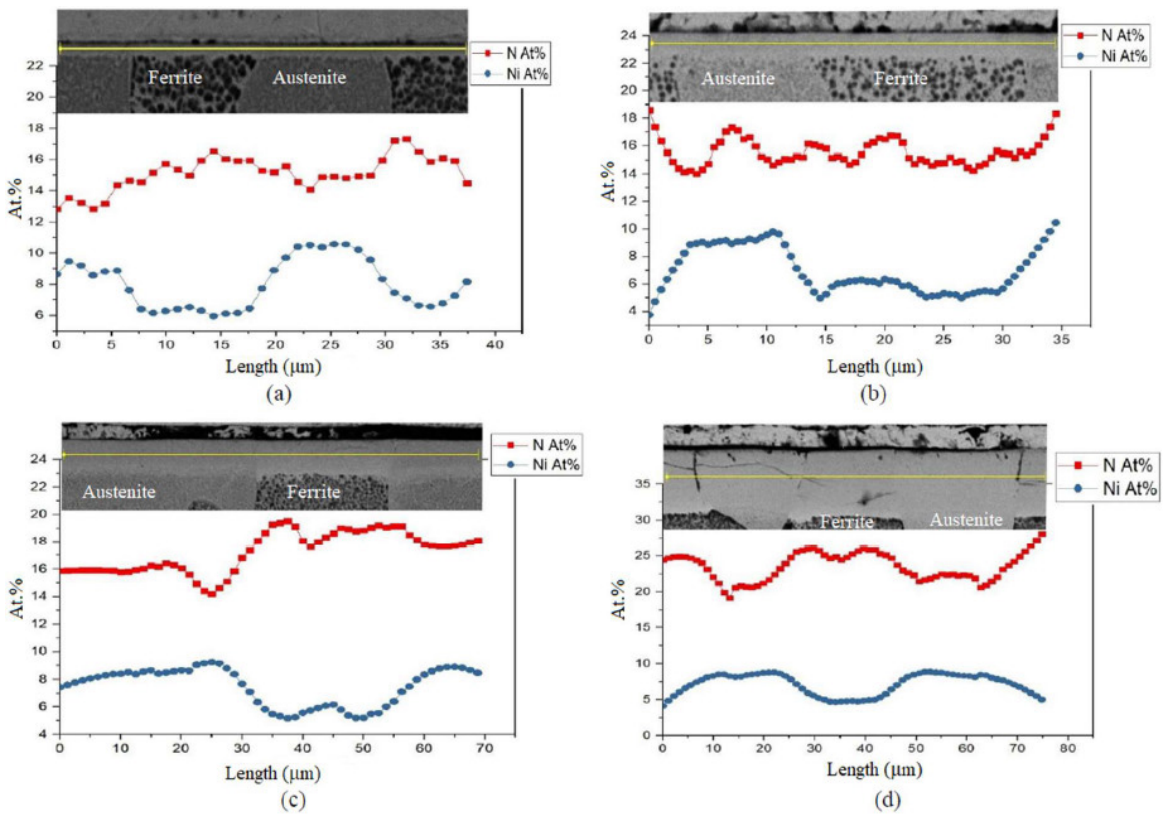


**Figure 4.** EDS nitrogen and nickel concentration line profile along the layer obtained for samples treated at: (a) 300, (b) 350, (c) 400, and (d) 450 °C. Treatments carried out for 4 h, using a gas mixture composed of 70% $N_2$ + 20% $H_2$ + 10% Ar at a flow rate of $3.34\times10^{-6}$ $Nm^3s^{-1}$, and pressure of 400 Pa.

residual stresses, displaced to smaller 2θ angles, confirm the crystalline lattice expansion caused by the nitrogen atoms alloying, as indicated in ref[17,50]. In addition to $\gamma_N$ peaks, samples treated at 300 and 350 °C also show original substrate peaks for both austenite and ferrite phases, which are no longer observed at 400 and 450 °C. The presence of original substrate peaks would indicate that the XRD probed depth is greater than the obtained layer thickness[51].

For all cases studied here, the obtainment of nitrogen-expanded ferrite cannot be assured from our XRD results (see Figure 3), giving additional support for the single-phase $\gamma_N$ layer assumption, and agreeing with the notion that nitrogen is a strong austenite stabilizer and substitutional diffusion is effectively frozen at the paraequilibrium temperatures [48]. In addition, it is possible to verify the existence of less intense peaks near the original austenite (γ) phase peaks, which could be attributed to a secondary nitrogen-expanded austenite phase layer, which is indicated as $\gamma'_N$[52]. A double layer comprising a double-structure nitrogen-expanded austenite layer was also recently observed in Toscano et al.[53]. According to Toscano et al.[53], the occurrence of this phase indicates the formation of nitrogen-expanded austenite layer with double structure, namely an outermost layer with a higher nitrogen content (varying on the 20-26 at.% N range) and an sublayer with lower nitrogen content (varying on the 4-10 at.% N). From Williamson et al.[54], it is stated that the $\gamma'_N$ phase formation is caused by stress-assisted diffusion, but here it could be also related to the just transformed ferrite between the outermost $\gamma_N$ phase layer and the non-chemically altered substrate bulk. The suggested ferrite-to-austenite transformation in the nitrogen-enriched layer in the present work could occur from the mechanism presented by Zangiabadi et al.[48] comprising the martensitic austenite formation, as well as by Forgas et al.[55], which proved this transformation to occur by reverse strain-induced martensitic transformation for a DSS. Being of interest of the reader, major details of these mechanisms can be found in ref[48,52,55-58].

Finally, still from Figure 3 results, it is possible confirming that the higher nitriding temperature the greater is the $\gamma_N$ peaks displacement to smaller angles, evidencing the higher nitrogen supersaturation of the obtained layer, which is in agreement with the EDS analysis presented in Figure 4a-d. Considering the possible sensitization observed in Figure 1d (and also Figure A1d, suggesting Cr-nitride phase precipitation, the absence of nitride phase peaks in the XRD pattern of samples treated at 450 °C would be due to the supposed small volumetric fraction of the formed nitride phase, being not detected with the applied XRD parameters.

EDS nitrogen and nickel elemental analysis longitudinally performed in the mean depth of the layer formed at 300, 350, 400 and 450 °C on both steel phases, regarding the original ferrite and austenite grains, exhibited average 15, 16, 17 and 23 at.% N (4.3, 4.6, 4.9 and 7.0 wt.% N) contents, respectively (see Figure 4a-d). Note that nickel content measurements agree well with the expected partition of this element in each phase, showing higher contents in austenite and smaller contents in the ferrite phase. In addition, results indicate the tendency of the nitrogen content in the layer to be higher in the layer formed over ferrite than in austenite phase, as mainly evidenced for samples treated at 400 and 450 C. This tendency is also related to the partition of the alloying elements in both steel phases. Higher amounts of chromium and molybdenum are evidenced in the ferrite grains, as presented in Table 2, which shows the nickel (austenite-stabilizer), and chromium and molybdenum (ferrite-stabilizer and stable nitride formers alloying elements) components partition on non-treated UNS S32750 SDSS samples. Using a variant of the Schaeffler diagram – the Kakhovskii constitutional diagram[59,60] – from the $Cr_{eq}$ (chromium-equivalent number) and $Ni_{eq}$ (nickel-equivalent number) estimation for the studied steel, only 0.66 wt.% N in solid solution would be enough to ensure the austenite phase stability. This limit nitrogen content value seems to be surpassed by far to the ones observed here, which showed a 4.3 wt.% N minimum as above-indicated, also agreeing well with the suggested ferrite-to-austenite transformation.

Microhardness measurement results for samples treated at the different studied temperatures are shown in Figure 5. Measurements were carried out in the layer formed on both the austenite and ferrite grains at the sample top (surface exposed to plasma) and bottom (surface non-exposed to plasma, thus untreated). Results indicate microhardness increase from 406 to 1900 $HV_{0.01}$ on ferrite grains and from 385 to 1530 $HV_{0.01}$ on austenite grains. Such microhardness increment is due to the high nitrogen supersaturation and the consequent compressive residual stresses generated by the expansion of the crystalline lattice in both phases, promoting increasing superficial hardening effect for higher nitriding temperatures, as observed by Tschiptschin et al.[8]. This result corroborates those presented in Figure 3, in which it was evidenced an increase in the $\gamma_N$ peaks displacement to smaller 2θ diffraction angles, indicating higher nitrogen supersaturation for higher treatment temperatures. In addition, the higher microhardness of the layer formed on ferrite phase is in agreement with its higher nitrogen concentration measured by EDS in this case, as shown in Figure 4a-d. The greater microhardness observed in the $\gamma_N$ layer formed on the ferrite grains is linked to its higher nitrogen content, since the higher partitioned chromium and molybdenum contents promote an intensified nitrogen attractiveness and trapping effect in the ferrite phase (see Table 2).

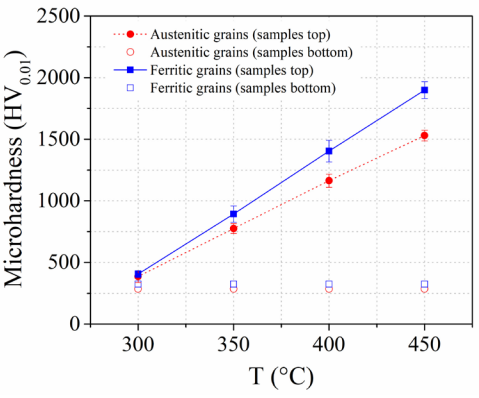


**Figure 5.** Surface microhardness for untreated sample and samples treated at 300, 350, 400 and 450 °C. Treatments carried out for 4 h, using a gas mixture composed of 70% $N_2$ + 20% $H_2$ + 10% Ar at a flow rate of $3.34\times10^{-6}$ $Nm^3s^{-1}$, and pressure of 400 Pa.

Regarding the actual layer microhardness value, it is worth mentioning that the indentation depth must not exceed 20% of the treated layer thickness to ensure that the measured microhardness values are significant and minimally affected by the non-chemically altered substrate bulk properties, as indicated in Borcz et al.[61]. So, the estimated increase on the microhardness by comparing the top and bottom surface values, above-mentioned, is strongly dependent on the obtained layer thickness. Note that for samples treated at 300 and 350 °C, the microhardness test indentation depth varied on the 0.66 to 1.38 μm range, comparable to the obtained layer thickness, which was on the order of 0.65 and 1.85 μm for both austenite and ferrite phases (see Figure 2). Differently, at 400 and 450 °C, obtained layers were thick enough to avoid the influence of the softer substrate bulk on the measured layer microhardness, in the case 4.35 ± 0.1 μm and 9.15 ± 0.1 μm, respectively, on both phases (grains).

### *3.2. Effect of the variation of the nitriding time*

Cross-section micrographs of samples treated at 350 °C for 2, 4 and 8 h are presented in Figure 6a-c, respectively (As an additional support optical micrographs are also presented in Figure A2a-c of Appendix A). The observed microstructures are similar to those presented in Figure 1a-c, with results also suggesting $\gamma_N$ phase layer formation on both austenite and ferrite phases. EDS nitrogen and nickel elemental analysis performed along treated layers exhibited average 13, 16 and 18 at. % N (3.6, 4.6 and 5.3 wt.% N) contents for samples treated for 2, 4 and 8 h (see Figure 7a-c, respectively). Taking into account the $Ni_{eq}$ and $Cr_{eq}$ values from the Kakhovskii constitutional diagram[47,59], such nitrogen contents also result to an austenite structure. Regarding the variation of the nickel contents for different steel phases, results were similar to those obtained in Figure 4a-d. For all studied treatment times,

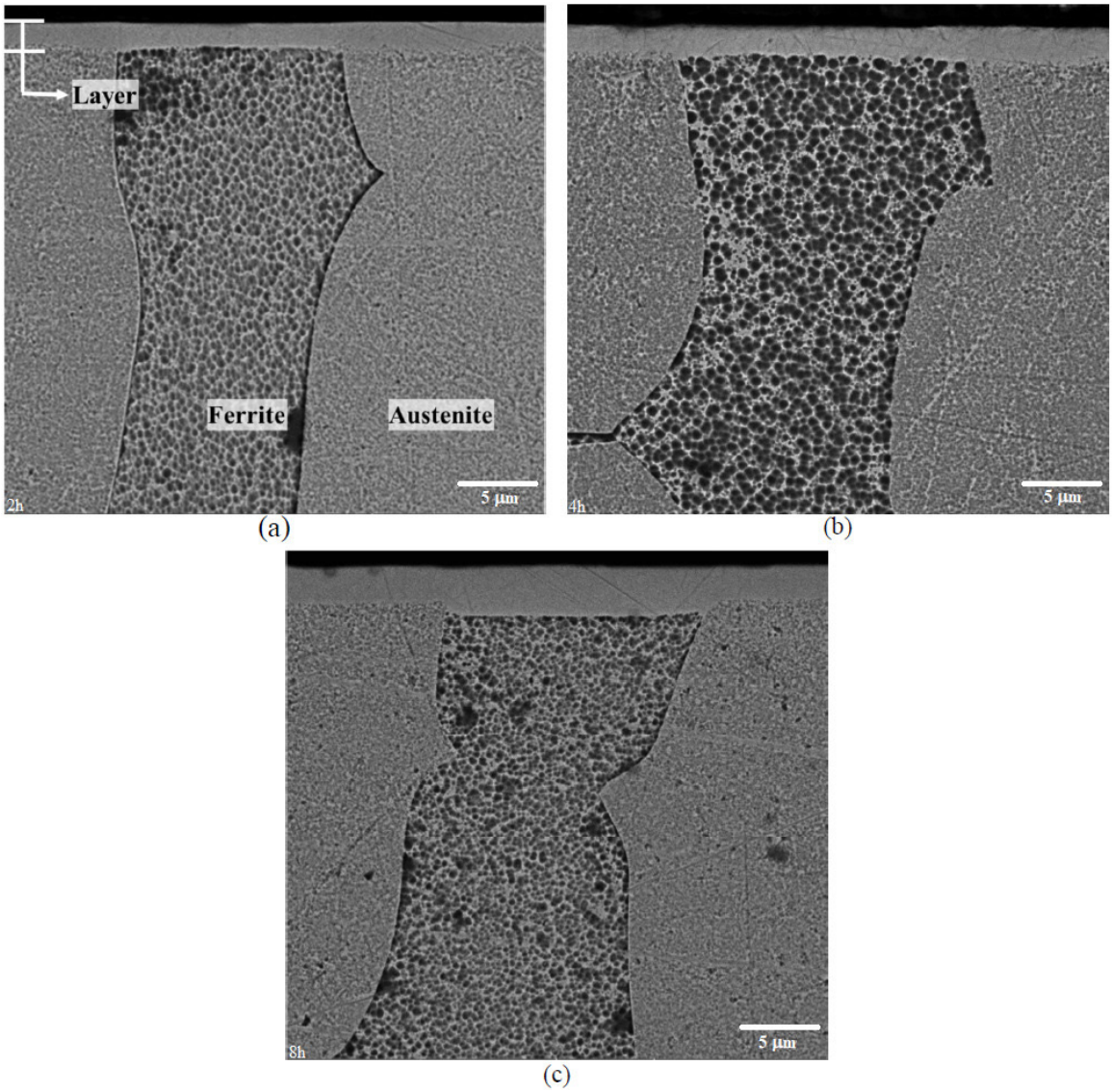


**Figure 6.** Cross-section SEM micrographs of samples treated at 350 °C for: (a) 2, (b) 4; and (c) 8 h. Treatments carried out using a gas mixture composed of 70% $N_2$ + 20% $H_2$ + 10% Ar at a flow rate of $3.34\times10^{-6}$ $Nm^3s^{-1}$, and pressure of 400 Pa.

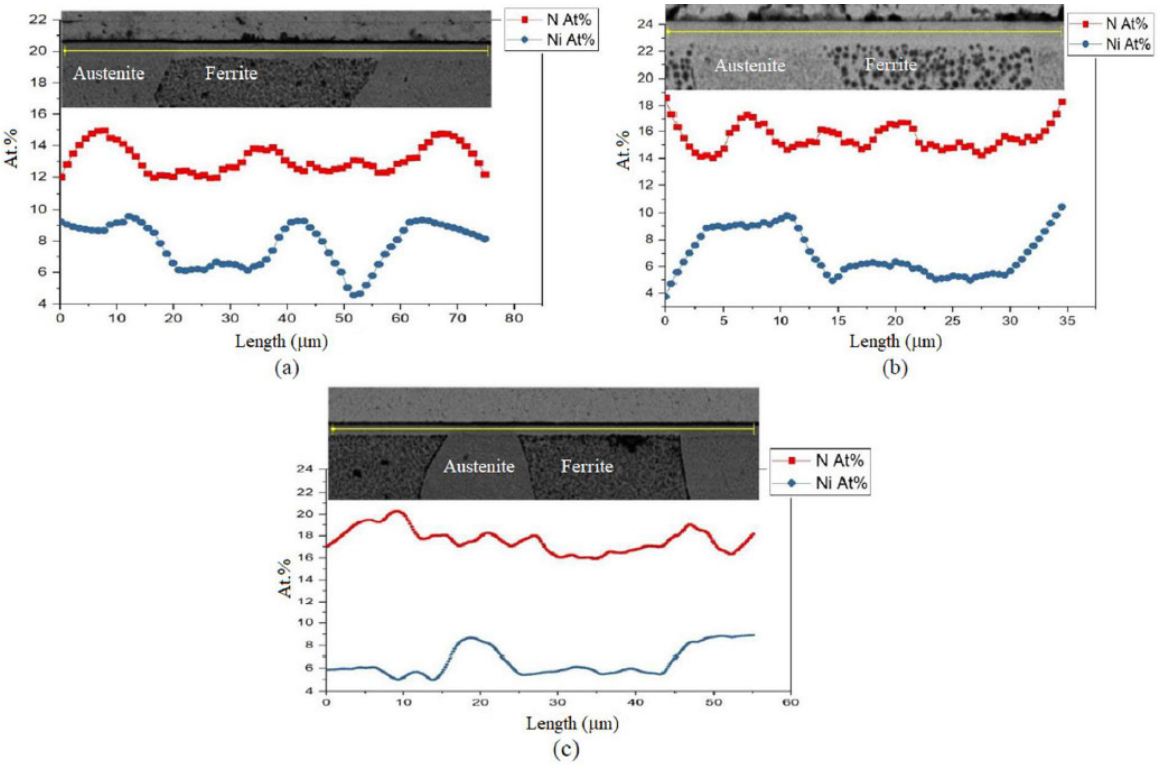


**Figure 7.** EDS nitrogen and nickel concentration line profile along the layer obtained for samples treated for: (a) 2, (b) 4, and (c) 8 h. Treatments carried out at 350 °C, using a gas mixture composed of 70% $N_2$ + 20% $H_2$ + 10% Ar at a flow rate of $3.34\times10^{-6}$ $Nm^3s^{-1}$, and pressure of 400 Pa.

there is no evidence of sensitization in the obtained layers, indicating that the Cr nitride precipitation did not occur.

A plot of the layer thickness values as a function of the square root of the treatment time resulted in a linear relationship (Figure 8), confirming that the nitrogen transport into the treated steel surface is diffusion-controlled. Figure 8 analysis shows that, considering the standard deviation of the layer thickness values, lines can be fitted cross the origin point (abscissa x = 0, and ordinate y = 0)[2], suggesting that no incubation period is presented for the treated layer formation. From this result, it can be inferred that the adopted plasma sputter-cleaning stage was able to promote the complete native oxide layer removal, which acts as a barrier preventing the nitrogen diffusion into the steel surface. It also indicates that the treated layer formation/growth occurred in the initial treatment periods for both substrate phases. Still, from Figure 8, at the specific processing temperature of 350 °C, the nitrided layer growth on the austenitic and ferritic grains can be described, from the nitriding time – *t*, by the Equations 4 and 5, respectively:

$$\ln \xi\left(h/\mu m\right) = 0.995 \cdot t^{1/2} \quad (4)$$

$$\ln \xi\left(h/\mu m\right) = 1.004 \cdot t^{1/2} \quad (5)$$

[2] The straight line adjustment was performed by forcing its passage through the origin.

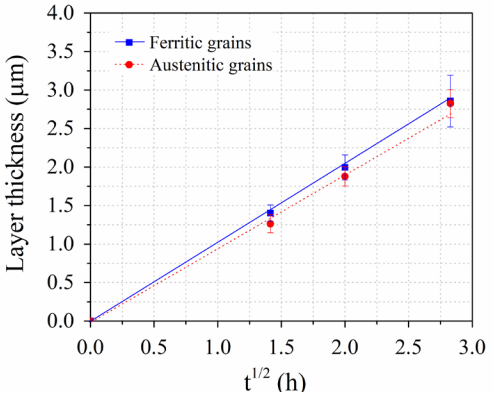


**Figure 8.** Layer thickness as a function of the square root of the treatment time for layer formed on austenite and ferrite grains of the UNS 32750 SDSS. Treatments carried out at 350 °C, using a gas mixture composed of 70% $N_2$ + 20% $H_2$ + 10% Ar at a flow rate of $3.34\times10^{-6}$ $Nm^3s^{-1}$, and pressure of 400 Pa.

Figure 9 shows XRD patterns obtained for samples treated at 350 °C for 2, 4 and 8 h. Results are similar to those obtained in the nitriding temperature series study, as previously shown in Figure 3. For all treatment times, original austenite phase peaks were also shifted to smaller 2θ angles, due to the high levels of nitrogen in solid solution, confirming the presence of nitrogen-expanded austenite ($\gamma_N$ / $\gamma'_N$) phase

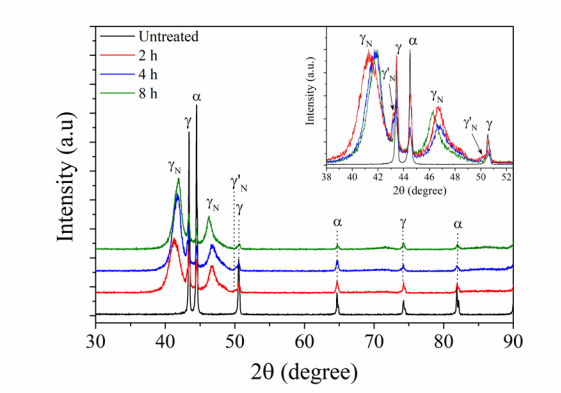


**Figure 9.** XRD patterns for untreated sample and samples treated at 350 °C for 2, 4 and 8 h. Treatments carried out using a gas mixture composed of 70% $N_2$ + 20% $H_2$ + 10% Ar at a flow rate of $3.34\times10^{-6}$ $Nm^3s^{-1}$, and pressure of 400 Pa. (where: γ – austenite phase; α – ferrite phase; $\gamma_N$ – nitrogen-expanded austenite phase; and $\gamma'_N$ – secondary nitrogen-expanded austenite phase.

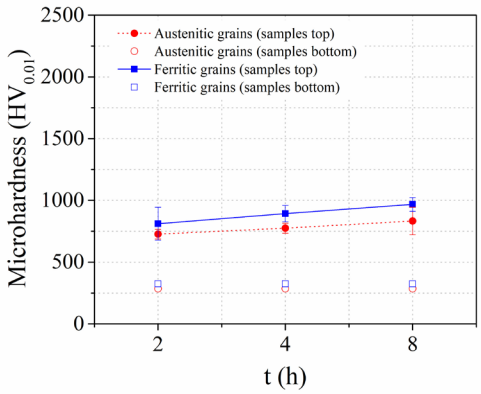


**Figure 10.** Surface microhardness for untreated sample and samples treated at 350 °C for 2, 4 and 8 h. Treatments carried out using a gas mixture composed of 70% $N_2$ + 20% $H_2$ + 10% Ar at a flow rate of $3.34\times10^{-6}$ $Nm^3s^{-1}$, and pressure of 400 Pa.

layer, being that no evidence of nitrogen-expanded ferrite phase peaks was observed. Finally, in XRD patterns details, the tendency of the major $\gamma_N$ phase peak to slightly shifting to greater angles with the increase of the treatment time was observed. This peak shift towards larger 2θ angles would suggest a possible relief of compressive residual stress in the treated material.

Figure 10 presents the microhardness measurements performed on treated and untreated surfaces. It is possible to note in both ferrite and austenite phases a slight layer microhardness increase as the nitriding time is increased. Layer microhardness values of 811, 893, and 968 $HV_{0.01}$ on ferrite grains, and 727, 775, and 833 $HV_{0.01}$ on austenite grains were obtained for 2, 4 and 8 h treated samples, respectively.

## 4. Conclusions

The effect of the treatment temperature and time on the microstructure, microhardness, and growth kinetics of layers produced by plasma nitriding in paraequilibrium conditions on UNS 32750 super duplex stainless steel samples was investigated. A deepened discussion comparing literature works on the present subject was performed, aiming to bring lights on the layer growth mechanism on the steel original austenite and ferrite phases from our results. The main conclusions for the studied conditions can be listed as follows:

- Low-temperature plasma nitriding can be successfully applied to improve surface microhardness of UNS 32750 SDSS, which is due to the formation of a single-phase $\gamma_N$ nitrided layer formed on both austenite and ferrite phase grains;
- For the treatment carried out at 450 °C microstructural results show significant evidences of incipient chromium nitride precipitation in the obtained layer and should be avoided since it will reduce the treated surface corrosion resistance, which is not acceptable for the case of stainless steels;
- The nitrogen diffusion in the studied SDSS surface, besides depending on each phase crystalline lattice structure, should also depend on at least four more factors: *i)* the partitioned alloying elements effect on each steel phase; *ii)* the distinct alloying elements trapping effect; *iii)* the generated (tensile in austenite, and compressive in ferrite) stress effect from thermal variations in the treatment beginning; and *iv)* the effect of the stresses arising from the transforming phases due to nitrogen supersaturation.
- Maximum microhardness of 1530 and 1900 $HV_{0.01}$ was obtained for the layer grown on austenite and ferrite phases, respectively.
- The nitrided layer growth kinetics is similar for both the austenite and ferrite steel phases, being compatible to that of a diffusion-controlled process. The calculated nitrogen diffusion activation energy was 115±3.2 $kJmol^{-1}$ and 120±5.4 $kJmol^{-1}$ for the treated layer formed on austenite and ferrite phase grains, respectively.

## 5. Acknowledgments

The authors wish to express thanks to the Laboratory of X-ray Optics and Instrumentation (LORXI-UFPR) and Electron Microscopy Center (CME-UFPR) for the use of the XRD and SEM equipment, respectively. This work was supported by CAPES - *Coordenação de Aperfeiçoamento de Pessoal de Nível Superior - Brasil* (Finance Code 001), Fundação Araucária do Estado do Paraná - *Brasil* (PRONEX - Grant N. 46744), CNPq - *Conselho Nacional de Desenvolvimento Científico e Tecnológico – Brasil*, CNPq-Universal Grant N. 482380/2012-8, and MCTI/CNPq/CT-Aquaviário Grant N. 456347/2013-5. Dr. C.J. Scheuer thanks to FAPERGS (Research Support Foundation of the *Rio Grande do Sul* State) by the financial support through Grant N. 19/2551-0001749-9.

## 6. References

1. Boillot P, Peultier J. Use of stainless steels in the industry: recent and future developments. Procedia Eng. 2014;83:309-21. http://dx.doi.org/10.1016/j.proeng.2014.09.015.

2. Knyazeva M, Pohl M. Duplex steels. Part II: carbides and nitrides. Metallogr. Microstruct. Anal. 2013;2(5):343-51. http://dx.doi.org/10.1007/s13632-013-0088-2.
3. Mandrino D, Donik C. Chemical-state information obtained by AES and XPS from thin oxide layers on duplex stainless steel surfaces. Vacuum. 2011;86(1):18-22. http://dx.doi.org/10.1016/j.vacuum.2011.03.025.
4. Chen M, Liu H, Wang L, Xu Z, Ji V, Jiang C. Investigation on the thermostability of residual stress and microstructure in shot peened SAF 2507 duplex stainless steel. Vacuum. 2018;153:145-53. http://dx.doi.org/10.1016/j.vacuum.2018.04.015.
5. Shang F, Wang Z, Chen X, Ji Z, Ren S, Qu X. UNS S32707 hyper-duplex stainless steel processed by powder injection molding and supersolidus liquid-phase sintering in nitrogen sintering atmosphere. Vacuum. 2021;184:109910. http://dx.doi.org/10.1016/j.vacuum.2020.109910.
6. Baldo S. Innovative steels for structural and corrosion resistance applications [dissertation]. Italy: University of Padua; 2010.
7. Pinedo CE, Varela LB, Tschiptschin AP. Low-temperature plasma nitriding of AISI F51 duplex stainless steel. Surf Coat Tech. 2013;232:839-43. http://dx.doi.org/10.1016/j.surfcoat.2013.06.109.
8. Tschiptschin AP, Varela LB, Pinedo CE, Li XY, Dong H. Development and microstructure characterization of single and duplex nitriding of UNS S31803 duplex stainless steel. Surf Coat Tech. 2017;327:83-92. http://dx.doi.org/10.1016/j.surfcoat.2017.08.018.
9. Bianco M, Poitel S, Hong J-E, Yang S, Wang Z-J, Willinger M, et al. Corrosion behaviour of nitrided ferritic stainless steels for use in solid oxide fuel cell devices. Corros Sci. 2020;165:108414. http://dx.doi.org/10.1016/j.corsci.2019.108414.
10. Bruna CE, Kurelo S, de Souza GB, Serbena FC, Lepienski CM, Borges PC. Mechanical properties and corrosion resistance of $\alpha_N$-rich layers produced by PIII on a super ferritic stainless steel. Surf Coat Tech. 2020;403:126388. http://dx.doi.org/10.1016/j.surfcoat.2020.126388.
11. Valencia-Alvarado R, de la Piedad-Beneitez A, de la Rosa-Vazquez J, López-Callejas R, Barocio SR, Godoy-Cabrera OG, et al. Nitriding of AISI 304 stainless steel in a 85% $H_2$/15% $N_2$ mixture with an inductively coupled plasma source. Vacuum. 2008;82(12):1360-3. http://dx.doi.org/10.1016/j.vacuum.2008.03.087.
12. Moskalioviene T, Galdikas A. Stress induced and concentration dependent diffusion of nitrogen in plasma nitrided austenitic stainless steel. Vacuum. 2012;86(10):1552-7. http://dx.doi.org/10.1016/j.vacuum.2012.03.026.
13. Nikolov K, Köster K, Kaestner P, Bräuer G, Klages C-P. Strip hollow cathode method for plasma thermochemical treatment for surface modification of thin metal strips: plasma nitriding of austenitic stainless steel sheets for bipolar plates. Vacuum. 2014;102:31-7. http://dx.doi.org/10.1016/j.vacuum.2013.11.001.
14. Lu S, Zhao X, Wang S, Li J, Wei W, Hu J. Performance enhancement by plasma nitriding at low gas pressure for 304 austenitic stainless steel. Vacuum. 2017;145:334-9. http://dx.doi.org/10.1016/j.vacuum.2017.09.020.
15. Yang D, Huang Y, Fan J, Jin M, Peng Y, Wang K. Effect of $N_2$ content in shielding gas on formation quality and microstructure of high nitrogen austenitic stainless steel fabricated by wire and arc additive manufacturing. J Manuf Process. 2021;161:261-9. http://dx.doi.org/10.1016/j.jmapro.2020.11.020.
16. Larisch B, Brusky U, Spies H-J. Plasma nitriding of stainless steels at low temperatures. Surf Coat Tech. 1999;116–119:205-11. http://dx.doi.org/10.1016/S0257-8972(99)00084-5.
17. Calabokis OP, Núñez de la Rosa Y, Lepienski CM, Cardoso RP, Borges PC. Crevice and pitting corrosion of low temperature plasma nitrided UNS S32750 super duplex stainless steel. Surf Coat Tech. 2021;413:127095. http://dx.doi.org/10.1016/j.surfcoat.2021.127095.
18. Bielawski J, Baranowska J. Formation of nitrided layers on duplex steel – influence of multiphase substrate. Surf Eng. 2010;26(4):299-305. http://dx.doi.org/10.1179/026708410X12593178265904.
19. Kliauga AM, Pohl M. Effect of plasma nitriding on wear and pitting corrosion resistance of X2 CrNiMoN 22 5 3 duplex stainless steel. Surf Coat Tech. 1998;9(1-3):1205-10. http://dx.doi.org/10.1016/S0257-8972(97)00240-5.
20. Blawert C, Mordike BL, Jirásková Y, Schneeweiss O. Structure and composition of expanded austenite produced by nitrogen plasma immersion ion implantation of stainless steels X6CrNiTi1810 and X2CrNiMoN2253. Surf Coat Tech. 1999;116–119:189-98. http://dx.doi.org/10.1016/S0257-8972(99)00086-9.
21. Li X, Dou W, Tian L, Dong H. Combating the tribo-corrosion of LDX2404 lean duplex stainless steel by low temperature plasma nitriding. Lubricants. 2018;6(4):93. http://dx.doi.org/10.3390/lubricants6040093.
22. Chiu LH, Su YY, Chen FS, Chang H. Microstructure and properties of active screen plasma nitrided duplex stainless steel. Mater Manuf Process. 2010;25(5):316-23. http://dx.doi.org/10.1080/10426911003748020.
23. Nagatsuka K, Nishimoto A, Akamatsu K. Surface hardening of duplex stainless steel by low temperature active screen plasma nitriding. Surf Coat Tech. 2010;205:S295-9. http://dx.doi.org/10.1016/j.surfcoat.2010.08.012.
24. Alphonsa J, Raja VS, Mukherjee S. Study of plasma nitriding and nitrocarburizing for higher corrosion resistance and hardness of 2205 duplex stainless steel. Corros Sci. 2015;100:121-32. http://dx.doi.org/10.1016/j.corsci.2015.07.014.
25. Assmann A, Foerster CE, Serbena FC, Lepienski CM, Chinelatto AL. Mechanical and tribological properties of LDX2101 duplex stainless steel submitted to glow discharge ion nitriding. IEEE Trans Plasma Sci. 2011;39(11):3108-14. http://dx.doi.org/10.1109/TPS.2011.2162344.
26. Blawert C, Weisheit A, Mordike BL, Knoop RM. Plasma immersion ion implantation of stainless steel: austenitic stainless steel in comparison to austenitic-ferritic stainless steel. Surf Coat Tech. 1996;85(1-2):15-27. http://dx.doi.org/10.1016/0257-8972(96)02880-0.
27. Oliveira WR, Kurelo BCES, Ditzel DG, Serbena FC, Foerster CE, Souza GB. On the S-phase formation and the balanced plasma nitriding of austenitic-ferritic super duplex stainless steel. Appl Surf Sci. 2018;434:1161-74. http://dx.doi.org/10.1016/j.apsusc.2017.11.021.
28. Bobadilla M, Tschiptschin A. On the nitrogen diffusion in a duplex stainless steel. Mater Res. 2015;18(2):390-4. http://dx.doi.org/10.1590/1516-1439.337714.
29. Tan H, Jiang Y, Deng B, Sun T, Xu J, Li J. Effect of annealing temperature on the pitting corrosion resistance of super duplex stainless steel UNS S32750. Mater Charact. 2009;60(9):1049-54. http://dx.doi.org/10.1016/j.matchar.2009.04.009.
30. Ferreira LM, Brunatto SF, Cardoso RP. Martensitic stainless steels low-temperature nitriding: dependence of substrate composition. Mater Res. 2015;18(3):622-7. http://dx.doi.org/10.1590/1516-1439.015215.
31. Sun Y. Kinetics of low temperature plasma carburizing of austenitic stainless steels. J Mater Process Technol. 2005;168(2):189-94. http://dx.doi.org/10.1016/j.jmatprotec.2004.10.005.
32. Anjos AD, Scheuer CJ, Brunatto SF, Cardoso RP. Low-temperature plasma nitrocarburizing of the AISI 420 martensitic stainless steel: microstructure and process kinetics. Surf Coat Tech. 2015;275:51-7. http://dx.doi.org/10.1016/j.surfcoat.2015.03.039.
33. Scheuer CJ, Cardoso RP, Mafra M, Brunatto SF. AISI 420 martensitic stainless steel low-temperature plasma assisted carburizing kinetics. Surf Coat Tech. 2013;214:30-7. http://dx.doi.org/10.1016/j.surfcoat.2012.10.060.
34. Scheuer CJ, Zanetti FI, Cardoso RP, Brunatto SF. Ultra-low to high-temperature plasma-assisted nitriding: revisiting and going

further on the martensitic stainless steel treatment. Mater Res Express. 2019;6(2):026529. http://dx.doi.org/10.1088/2053-1591/aaeca2.
35. Chiu LH, Su YY, Chen FS, Chang H. Microstructure and properties of active screen plasma nitrided duplex stainless steel. Mater Manuf Process. 2010;25(5):316-23. http://dx.doi.org/10.1080/10426911003748020.
36. Bielawski J, Baranowska J, Szczecinski K. Microstructure and properties of layers on chromium steel. Surf Coat Tech. 2006;200:6572-7. http://dx.doi.org/10.1016/j.surfcoat.2005.11.037.
37. Mendes AF, Scheuer CJ, Joanidis IL, Cardoso RP, Mafra M, Klein AN, et al. Low-temperature plasma nitriding of sintered PIM 316L austenitic stainless steel. Mater Res. 2014;17(Suppl suppl 1):100-9. http://dx.doi.org/10.1590/S1516-14392014005000064.
38. Menthe E, Rie K-T. Further investigation of the structure and properties of austenitic stainless steel after plasma nitriding. Surf Coat Tech. 1999;116-119:259-63. http://dx.doi.org/10.1016/S0257-8972(99)00085-7.
39. Wert C, Zener C. Interstitial atomic diffusion coefficients. Phys Rev. 1949;76(8):1169-75. http://dx.doi.org/10.1103/PhysRev.76.1169.
40. Cardoso RP, Scheuer CJ, Brunatto SF. Stainless steel: low-temperature nitriding kinetics. In: Colás R, Totten GE, editors. Encyclopedia of iron, steel, and their alloys. 1st ed. Boca Raton: CRC Press. 2016. Chapter 176; p. 2153-68. http://dx.doi.org/10.1081/E-EISA-120051669.
41. Grabke HJ, Petersen EM. Diffusivity of nitrogen in iron-nickel alloys. Scr Metall. 1978;12(12):1111-4. http://dx.doi.org/10.1016/0036-9748(78)90085-6.
42. Peng Y, Gong J, Chen C, Liu Z, Jiang Y. Numerical analysis of stress gradient and traps effects on carbon diffusion in AISI 316l during low temperature gas phase carburization. Metals. 2018;8(4):214. http://dx.doi.org/10.3390/met8040214.
43. Parascandola S, Möller W, Williamson DL. The nitrogen transport in austenitic stainless steel at moderate temperatures. Appl Phys Lett. 2000;76(16):2194-6. http://dx.doi.org/10.1063/1.126294.
44. Johansson J, Odén M, Zeng X-H. Evolution of the residual stress state in a duplex stainless steel during loading. Acta Mater. 1999;47(9):2669-84. http://dx.doi.org/10.1016/S1359-6454(99)00149-4.
45. Li W, Li X, Dong H. Effect of tensile stress on the formation of S-phase during low-temperature plasma carburizing of 316L foil. Acta Mater. 2011;59(14):5765-74. http://dx.doi.org/10.1016/j.actamat.2011.05.053.
46. Li W, Guo W, Zhu X, Jin X, Li X, Dong H. The effect of applied compressive stress on the diffusion of carbon in carbon supersaturated S-phase layer. Surf Coat Tech. 2017;331:1-6. http://dx.doi.org/10.1016/j.surfcoat.2017.10.035.
47. Allenstein AN, Cardoso RP, Machado KD, Weber S, Pereira KMP, dos Santos CAL, et al. Strong evidences of tempered martensite-to-nitrogen-expanded austenite transformation in CA-6NM steel. Mater Sci Eng A. 2012;552:569-72. http://dx.doi.org/10.1016/j.msea.2012.05.075.
48. Zangiabadi A, Dalton JC, Wang D, Ernst F, Heuer AH. The formation of martensitic austenite during nitridation of martensitic and duplex stainless steels. Metall Mater Trans, A Phys Metall Mater Sci. 2017;48A(1):8-13. http://dx.doi.org/10.1007/s11661-016-3853-4.
49. Ciuffini AF, Barella S, Di Cecca C, Gruttadauria A, Mapelli C, Mombelli D. Isothermal austenite–ferrite phase transformations and microstructural evolution during annealing in super duplex stainless steels. Metals (Basel). 2017;7(9):368. http://dx.doi.org/10.3390/met7090368.
50. Zhang L, Bell T. Structure and corrosion resistance of plasma nitrided stainless steel. Surf Eng. 1985;1(2):131-6. http://dx.doi.org/10.1179/sur.1985.1.2.131.
51. Borgioli F, Fossati A, Galvanetto E, Bacci T. Glow discharge nitriding of AISI 316L austenitic stainless steel: influence of treatment temperature. Surf Coat Tech. 2005;200(7):2474-80. http://dx.doi.org/10.1016/j.surfcoat.2004.07.110.
52. Zhang H, Pradeep KG, Mandal S, Ponge D, Raabe D. New insights into the austenitization process of low-alloyed hypereutectoid steels: nucleation analysis of strain-induced austenite formation. Acta Mater. 2014;80:296-308. http://dx.doi.org/10.1016/j.actamat.2014.07.073.
53. Toscano TD, Cardoso RP, Brunatto SF. A novel concept of hybrid treatment for high-hardenability steels: concomitant hardening and paraequilibrium thermochemical treatment to produce interstitially-hardened/stabilized-austenite surfaces. Steel Res Int. 2020;91(10):2000189. http://dx.doi.org/10.1002/srin.202000189.
54. Williamson DL, Davis JA, Wilbur PJ. Effect of austenitic stainless steel composition on low-energy, high-flux, nitrogen ion beam processing. Surf Coat Tech. 1998;103–104:178-84. http://dx.doi.org/10.1016/S0257-8972(98)00389-2.
55. Forgas A Jr, Marangoni J, Otubo J, Donato GHB, Magnabosco R. Reverse strain-induced martensitic transformation of the ferrite to austenite in duplex stainless steels. J Mater Sci. 2016;51(23):10452-63. http://dx.doi.org/10.1007/s10853-016-0265-1.
56. Southwick PD, Honeycombe RWK. Decomposition of ferrite to austenite in 26%Cr-5%Ni stainless steel. Met Sci. 1980;14(7):253-61. http://dx.doi.org/10.1179/030634580790426418.
57. Maclaren I, Ivanisenko Y, Valiev RZ, Fecht HJ. Reverse martensitic transformation of ferrite to austenite under severe plastic deformation. J Phys Conf Ser. 2006;26:335-8. http://dx.doi.org/10.1088/1742-6596/26/1/081.
58. Ivanisenko Y, Maclaren I, Sauvage X, Valiev RZ, Fecht HJ. Shear Induced α–γ transformation in nanoscale Fe-C composite. Acta Mater. 2006;54(6):1659-69. http://dx.doi.org/10.1016/j.actamat.2005.11.034.
59. Lippold JC, Kotecki DJ. Welding metallurgy and weldability of stainless steels. Hoboken: John Wiley & Sons; 2005.
60. Reis RF, Maliska AM, Borges PC. Nitrogen surface enrichment of austenitic stainless steel ISO 5832-1. J Mater Sci. 2011;46(3):846-54. http://dx.doi.org/10.1007/s10853-010-4827-3.
61. Borcz C, Lepienski CM, Brunatto SF. Surface modification of pure niobium by plasma nitriding. Surf Coat Tech. 2013;224:114-9. http://dx.doi.org/10.1016/j.surfcoat.2013.03.008.

## Supplementary material

The following online material is available for this article:
Appendix A